Engineering Journal of Qatar University, Vol. 5, 1992, p. 95 - 117

CONVECTION IN A ROTATING FLUID OVER A SLOPING BOTTOM, WITH APPLICATION TO THE ARABIAN GULF

Khalid R. Al-Hajri*, Shenn-Yu Chao* and Timothy W. Kao***
*Department of Civil Engineering, University of Qatar, Doha.
**Horn Point Environmental Laboratory, University of Maryland, Cambridge, Maryland.
***Department of Civil Engineering, The Catholic University of America, Washington, D.C.

ABSTRACT

Convective motions over a sloping bottom driven by evaporation and freshening are investigated by integrating the complete momentum and mass conservation equations. The problem is posed as an initial value problem in a rotating frame of reference to study the dynamics of establishment of the quasi-steady state circulation when the rate of increase of density due to evaporation is equal to the rate of decrease of density due to freshening. The study is motivated by an attempt to give a description of the sub-mesoscale vertical convection in the cross-shore plane of an enclosed elongated basin such as the Arabian Gulf where these physical mechanisms are operative. The effect of the addition of wind-forcing in the longshore direction is also investigated. To resolve sub-mesoscale phenomena we find it necessary to employ a model basin which is smaller in its horizontal dimension than the Arabian Gulf. The results of the two dimensional model are presented herein. These results include (i) a detailed description of the evaporative-convective adjustment process; (ii) a measure of the convective length scale and vertical velocity; (iii) an assessment of the relative strengths of the buoyancy induced geostrophic current in the alongshore direction and the direct wind induced velocities; (iv) an assessment of the effect of wind on the density structures and (v) an analogy between the forcing by diffusive buoyant source and advective buoyant source.

INTRODUCTION

Surface sources of negative buoyancy and the resulting convective motions are important in problems of geophysical interest. A notable example is found in the large evaporation rate over the Arabian Gulf and the Red Sea.

The Gulf is a 990 km long semi-enclosed shallow sea which has an average width of about 250 km, a mean depth of 36 m and a maximum depth of about 100 m (see Fig. 1). The bathymetry of the basin is markedly asymmetrical across its axis. Its floor on the Iranian side is relatively deep and steep, while that on the Arabian side is shallow and slopes gently toward the bathymetric axis (Purser, 1973).

The Gulf is a land-locked sea with a strong negative water balance, evaporation (1.44 m/yr) far exceeds the total input of fresh water from precipitation (0.07 m/yr)

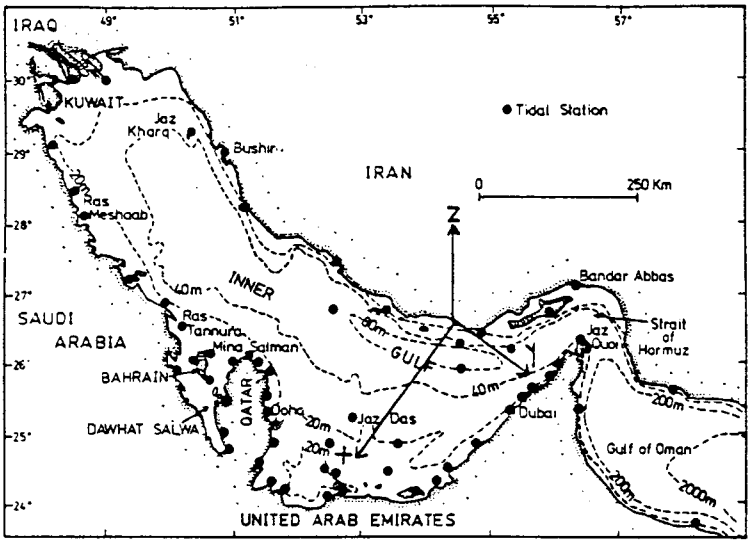

Fig. 1: The coordinate system of the 2-D model on a map of the Arabian Gulf.

and river discharge (0.07 m/yr). Throughout the year, relatively low-salinity surface water from the Gulf of Oman enters the Gulf through the Strait of Hormuz and flows northwestward along the Iranian coast against the prevailing wind which is northwesterly throughout the year (average wind speed = 5 m/s). The freshening water mass undergoes transformation in the progress nothwards, but it can be coherently identified at least to the mid-length cross-section of the Gulf (Brewer *et al,* 1978).

With the understanding of the sub-mesoscale transverse motions in the cross-shore section plane of the Gulf as a motivation, we undertake to investigate convective adjustment process over a sloping bottom, driven by evaporation and freshening, through a two-dimensional model using the complete Navier-Stokes and diffusion equations in a rotating frame of reference. The problem is posed as an initial-boundary value problem to study the dynamics of establishment of the quasi-steady state circulation when the rate of increase in density due to evaporation is equal to the rate of decrease of density due to freshening. The negative convection generates flows with horizontal length scales of 100 m or less, which is more than three order or magnitude smaller than the width of the Gulf. To preserve these sub-mesoscale phenomena, the horizontal dimension of the basin is made much smaller than that of the Gulf. The model is therefore more applicable to the shallow reaches of the Gulf, where the denser water is generated. In the three-dimensional study, Al-Hajri, *et al,* 1991, the actual dimensions of the Gulf will be employed, but the coarse resolution truncates the sub-mesoscale motion.

Thus, the present work can be regarded as the sub-mesoscale complement of the 3-D model.

If the deepest depth of the cross-section is denoted by d, the coriolis parameter by f, the reduced gravity due to a representative density anomaly by g', kinematic (eddy) viscosity by ν, we can form a velocity scale U by (fd). The dimensionless parameters of the problem are then the "thermal" Rossby Number ($g'd/U^2$) and the Reynolds number $Re=Ud/\nu$. In this study we will assume that the eddy diffusivity D is equal to the eddy viscosity so that the Schmidt Number Sc is equal to unity. In the geophysical context of the present study, the thermal Rossby number is very large ($>10^3$) and Re is of order 10^2. The range of parameters studied here is markedly different from those covered by Quon (1987) in a numerical study of thermal convection of a rotating differentially heated unit square. The thermal Rossby number is his study is very small (<1), Reynolds number is 10^4, and Schmidt number is 10.

In this paper, we will present the results of the two dimensional model which has the following objectives:

(i) to examine the evaporation induced convection process in a cross-section with sloping bottom.

(ii) to establish the horizontal length scale and vertical velocity scale of the associated motion;

(iii) to establish the relative strengths of thermal-wind and direct wind induced velocities in the along-shore direction.

(iv) to establish the analogy between forcing by buoyant (fresher) water inflow (forced convection) and by diffusive buoyant source (free convection). This analogy will be exploited in the three-dimensional model in the subsequent paper on the three-dimensional general circulation of the Gulf.

DESCRIPTION OF THE MODEL

The model is based on the numerical integration of the full Navier-Stokes and diffusion equations in the vertical cross-section plane. It is two-dimensional in x-z plane, and assumes no variations in y-direction. The model basin and the coordinate system (x,y,z) is shown in Fig. 2. For application to the Gulf, the idealized vertical section is oriented such that the Iranian side on the left of the section, looking in the positive y-direction toward the Strait. Since all length scales are non-dimensionalized in the model, the depth d can be chosen as a characteristic depth scale for the shallow reaches of the Gulf.

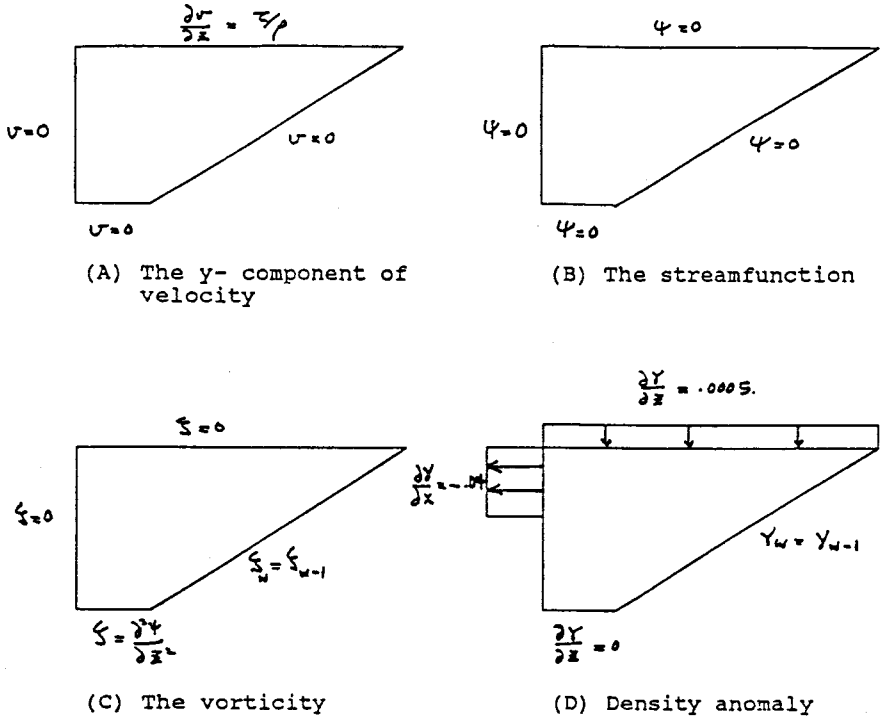

Fig. 3: Boundary conditions for the model.

where x and $\overline{x}$ are the original and transformed coordinate, respectively. The value of b is chosen as 0.2. Thus $\overline{x}$ varies from 0 to 1 as x varies from 0 to ∞. The z-coordinate is unstreched. Then the stretched form of the governing equations and the boundary conditions are written in a finite difference form. The central difference in space and the forward difference in time are used except the non-linear terms, for which the special three-point noncentral method is used (Torrence and Rocket, 1968). Details of the transformation and the finite difference equations can be found in Kao, *et al*, 1978.

RESULTS OF THE MODEL

a. Cross-shelf structure:

The cross-shelf density-driven circulation with the associated alongshore current is investigated here. The density-driven experiment is driven by buoyancy flux: positive buoyancy forcing at the upper vertical wall and negative buoyancy forcing

at the sea surface. The former represents the freshening process from the deeper side of the basin and the latter represents evaporation. Steady-state is achieved through frictional and diffusive geostrophic adjustment in 7 days. The steady-state solution of the density distribution is shown in Fig. 4. Along the deeper side, the density structure shows the light water pool produced by the buoyancy flux is trapped at the coast by rotation.

The isopycnals of the freshwater defined by the negative density anomaly extend from the sea surface and intersect the left hand wall. On the shallow shelf, evaporation generates heavy water (higher salinity) that travels down along the slope toward the deep portion of the section. The isopycnals of the dense water defined by the positive density anomaly originate at the sea surface and extend parallel to the sloping shelf toward the deeper side. It should be noted that the dense water covers a large portion of the cross-section, indicating the importance of evaporation in the cross-shelf dynamics. This density structure is in general agreement with that of field observations of Brewer, *et al,* 1978. Fig. 5 shows the most detailed transverse salinity section of Brewer survey. It is located on the transect along the x-axis of Fig. 1, with Iran on the right of the section. Sugimato and Whitehead (1983) conducted laboratory experiments to simulate convective flows in a shallow rectangular sea of constant depth which adjoined a deep ocean through a uniformly sloping bottom region. The experiment is cooled from above and heated through the offshore side. Their cross-shore isothermal pattern is similar to that of the density structure of Fig. 4. In their experiment, the thermal

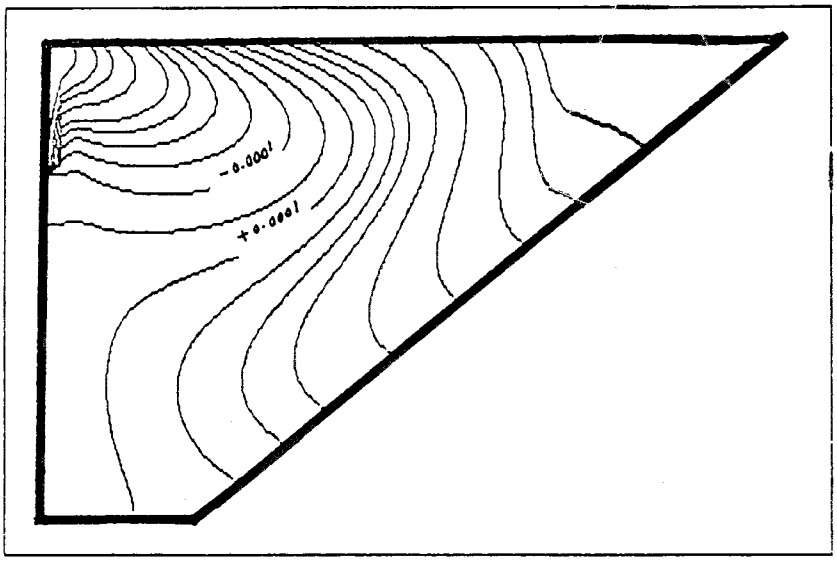

Fig. 4: Isopycnals for the density-driven case at steady-state ($\Delta\rho$ = .0001)

front is trapped by rotation near the heated wall. The cold water is formed at the surface of the coastal zone and sink to the bottom along the slope.

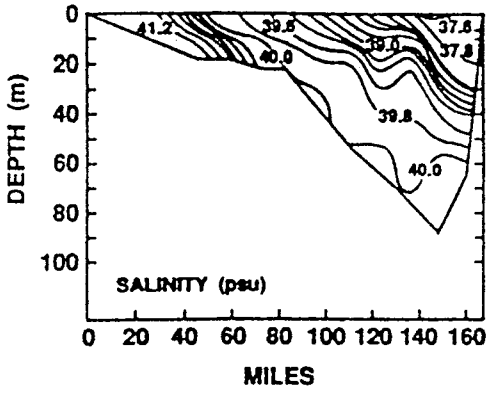

Fig. 5: Vertical salinity section across the Gulf on the transect along the x-axis of Fig. 1 Iran is to be right (After Brewer *et al*, 1978).

The contours of the isotachs of the alongshore velocity corresponding to Fig. 4 are given in Fig. 6. A surface jet stream is established in the negative y- direction, where the density gradient is maximum on the sloping shelf. The sinking motion of the dense water along the slope, therefore, is arrested by geostrophy. The geostrophic balance is between the presence gradient due to cross-shelf density variation and Coriolis force. On the deeper side of the section, a weaker return flow is present. It is seen that the along-shore velocity due to thermal-wind effect and the bulk of the associated transport is directed in the negative y-direction. The maximum surface velocity of the thermal wind velocity is less than 1 cm/sec., which is weak. The thermal-wind effect is therefore easily overwhelmed by direct wind induced velocity. This will be examined in the next section.

The cross-stream circulation is shown in Fig. 7. It is dominated by a laminar convection cell with upwelling over the deeper basin and downwelling over the shallow shelf. The cross-sectional extent of this convection cell is about 6 d in the model. It is comparable to the internal Rossby radius of deformation L_D which can be found from the relation:

$$L_D = \overline{N}d/f,$$

where $\overline{N}$ is the averaged buoyancy frequency of the model taken about 2d from the deep side ($\overline{N}\sim(10^{-3}/s)$), f is Coriolis parameter, ($f=10^{-4}$) and d is the vertical scale.

The above formula yields a baroclinic Rossby radius of deformation of about 10d. This suggests that the convection cell is dominated by rotation.

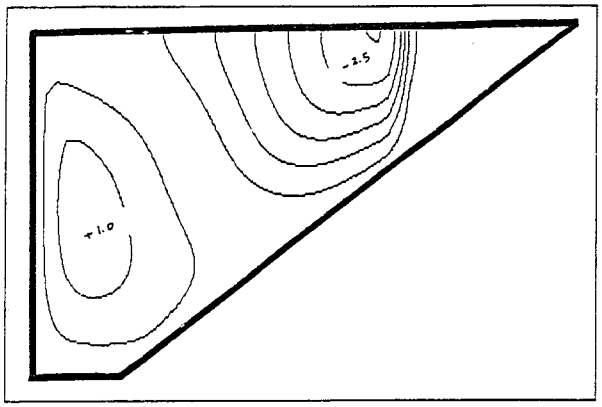

Fig. 6: Isotachs of the alongshore velocity, for the density driven case ($\Delta v = 0.5$).

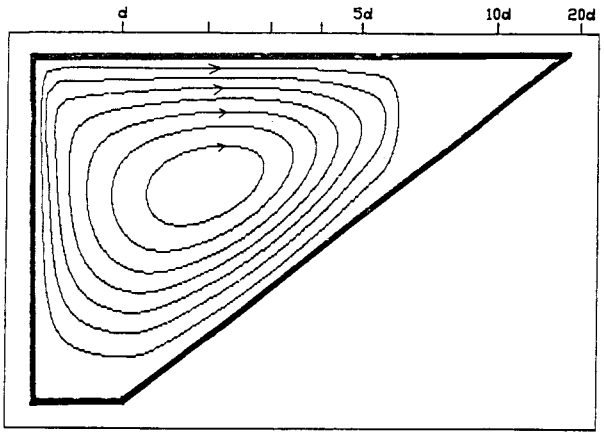

Fig. 7: Streamlines for the density-driven case ($\Delta\psi = 0.1$).

In order to investigate the effect of the bottom-slope topography, a flat bottom case is compared with the sloping bottom topography, where all parameters are the same except for the bottom topography. The density structure of the uniform depth case at t = 7 days is shown in Fig. 8. At t = 7, the flow has reached steady-state equilibrium.

The most significant effects of the sloping shelf is on the formation of the dense water. The fresher water due to freshening is persistent as in the sloping bottom case. The density structure of the dense water in this case shows a number of isopycnals that extend from top to bottom to the right of the freshening source, followed by a series of a sinking plumes of heavier water generated by evaporation.

It is clear that the sloping topography acts as a slide for the dense water that forms over the shallows. It then slides down the slope as a dense gravity current toward the deeper channel underneath the freshwater and is eventually arrested through geostrophy. This phenomenon has obvious implications to the shortening of the flushing time of the Gulf.

The associated streamlines pattern for the flat bottom case is shown in Fig. 9. The large convection cell is dominated by rotation as seen earlier. The smaller cells are controlled by evaporative convection and their horizontal extent is governed by evaporative convection and their horizontal extent is governed by the depth of the basin.

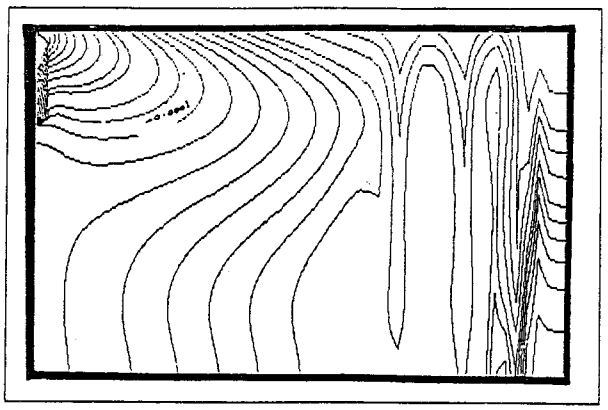

Fig. 8: Isopycnals for the density-driven case with a flat bottom ($\Delta\omega = 0.0001$).

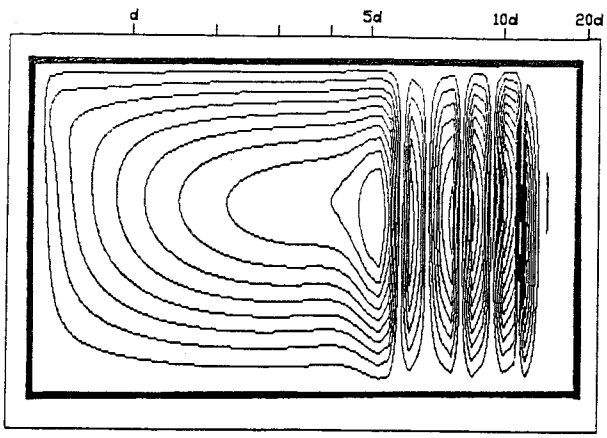

Fig. 9: Streamlines for the density-driven case with a flat bottom ($\Delta\psi = 0.01$)

b. Wind effects:

To investigate the wind effects on the dynamics of the cross shelf circulation, a surface wind stress is added to the surface boundary condition for the y- component of the velocity once the equilibrium solution is reached in the previous experiment. The surface stress is represented as $\nu\ \partial v/\partial z = \tau/\rho$ for the condition of wind stress, τ. The wind stress is usually represented by a surface friction velocity given by $u_*^2 = \tau/\rho_a$, where u_* is the friction velocity and ρ_a is the air density. The surface friction velocity is about 18 cm/s for the average wind speed prevailing over the Gulf region.

Since the predominant wind in the Gulf is from the northwest, the model wind stress is in the positive y- direction. In this experiment, the wind stress is applied uniformly to the surface for six days after the steady state solution is reached in the previous run. During this period, the freshening process and evaporation are not relaxed. The density field, streamliness pattern, and the v- component at t = 13 are shown in Figs. 10, 11 and 12, respectively. Salient features induced by the wind are summarized as follows:

1. The wind in the positive y- direction enhances the clockwise transverse circulation pattsern shows a convection cell which is expanded toward the shallow shelf by the wind as shwon in Fig. 11.

2. The density distribution of Fig. 4 is only midly affected by the wind field. The isopycnals expand in the direction of the surface Ekman flow. This feature is common with the two dimensional models of Ikeda (1985) and Porter (1986), although the cross-section geometry in these two models is different from the present model. The dense water formed by evaporation sinks further along the sloping topography in the presence of wind forcing. This feature is noticed in the

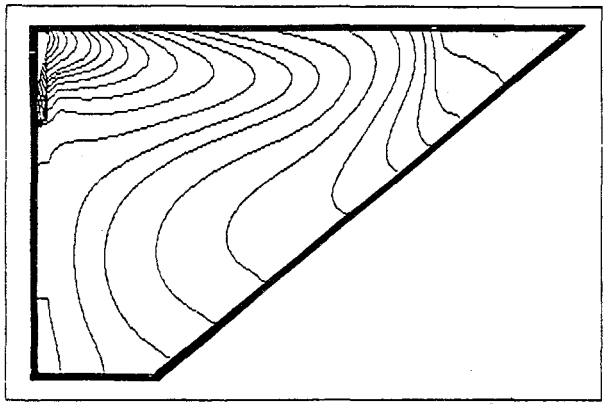

Fig.10: Isopycnals at t = 13 for the case driven by both density and wind($\Delta\rho$ = .0001)

beginning time of convection, and the convection process depend on Froude number. Cases #1 and #2 are stable, case #3 is stable initially then becomes unstable at a later time.

Case #4, the most unstable case, is discussed here. The onset of convective instability starts very early (t=0.4), within hours after evaporation starts. The cellular motion initially appears at the top layer on the deep side of the section as shown in Fig. 13. The convection in this case is vigorous, penetrating downward and horizontally to the right.

The streamline pattern for t = 0.4 is shown in Fig. 14. The cellular convection in the convection regime altered the isopycnal profile dramatically. The wavelength at

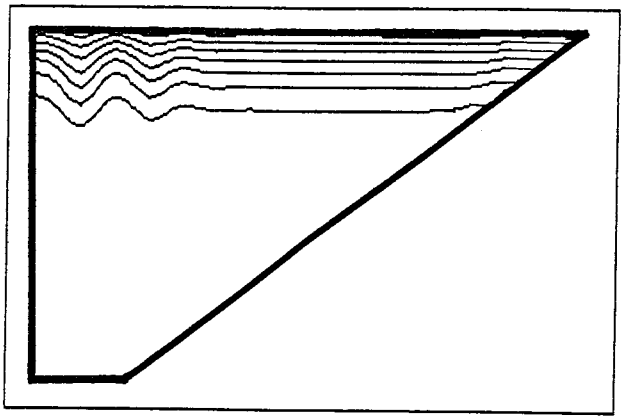

Fig. 13: Isopycnals for the uniform evaporation case at t = 0.4 for case 4 ($\Delta\rho$ = .0001)

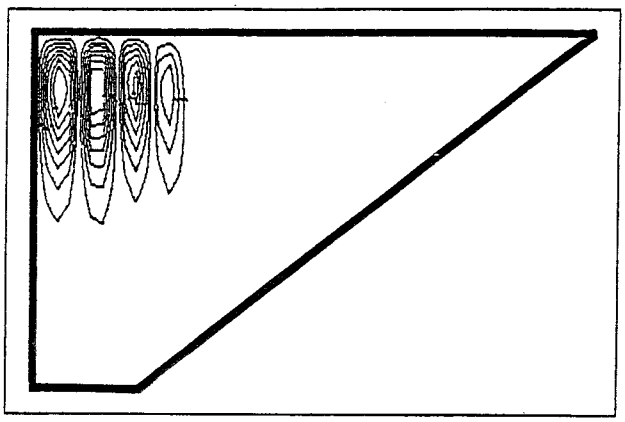

Fig. 14: Streamlines for the uniform evaporation case at t = 0.4 for case 4 ($\Delta\psi$ = 0.1)

the start of the convection is about twice the depth. The induced vertical velocity is strong, on the order of 10^{-1} cm/s. As Froude number is decreased, the buoyancy is increased, thus, the baroclinic term, $\partial\gamma/\partial x$, in the vorticity equation is enhanced, which in turn, produces a strong vertical velocity.

It should be noted here that the initial appearance of instability on the deep side of the basin and initial wavelength of unstable waves are not affected by the stretched coordinate. Quite a few experiments described here are repeated in the unstretched coordinate. Results are very similar.

At t = 2.0, the wavy isopycnals are shifted toward the right. Fig. 15 shows this trend in the displacement of the sinking plumes to shallow side of the basin. This seems to be related to the rotational effect that causes the interaction and coalescence of modes, producing an organized cell of which the horizontal extent is on the order of the internal Rossby radius of deformation. The streamline pattern of Fig. 16 is consistent with this trend. One large cell is being formed on the deep side of the section with downwelling on the shallow shelf. The critical Rayleigh number for this case is about 2300. It is based on an internal length scale (ℓ) such as the height of the top convective layer rather than the total depth of the cross-section (Quon, 1987). The top, unstable layer, ℓ, at the onset of convection for this case is about 0.1d. Howard (1966) estimated a comparable critical Rayleigh number at the onset of thermal instability for a deep layer of fluid without rotation, heated from below. It seems that at times less than the inertial period, the adjustment is approximately the same as in a non-rotating system.

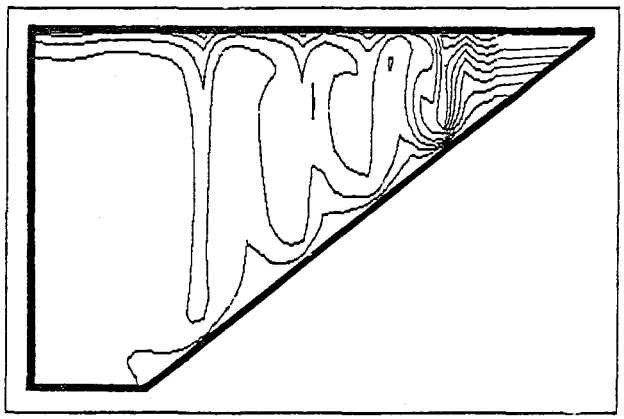

Fig. 15: Isopycnals for the uniform evaporation case at t = 2.0 for case 4 ($\Delta\rho$ = .0001)

$$W^* = k\ ((\Delta\rho/\rho_o)\ gd\ )^{1/2}$$

The slope of W* versus 1/F as determined from Table 1 and other like experiments not reported here is about 10^{-5}. Therefore;

$$W^* = 10^{-5}((\Delta\rho/\rho_o)\ gd\ )^{1/2}$$

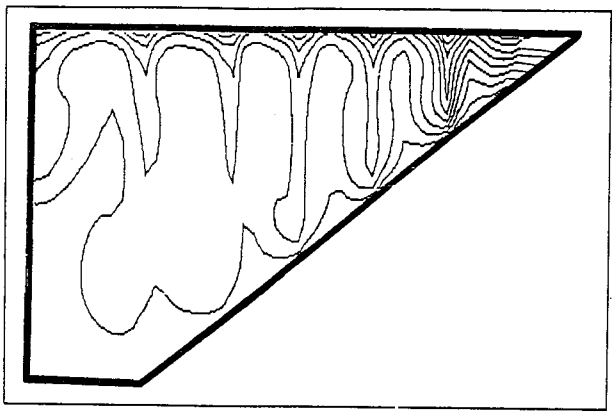

Fig. 19: Isopycnals for the perturbed evaporation case at t = 1.0 for case 4 ($\Delta\rho$ = .0001)

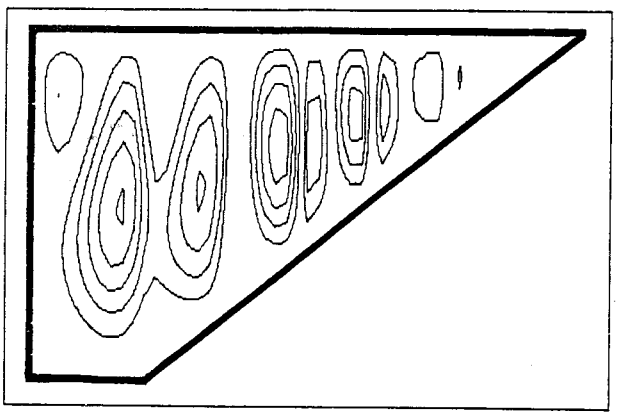

Fig. 20: Streamlines for the perturbed evaporation case at t = 1.0 for case 4 ($\Delta\psi$ = 0.1)

It is obvious from this relation that the vertical velocity is proportional to the strength of the buoyancy. There is, of course, a small uncertainty in this relationship that comes from determining the proportionality constant and in estimating the buoyancy term. The dependence of W* on other dimensionless parameters are much weaker.

d. The analogy between light water inflow and mass diffusion

The freshening process can be simulated by imposing buoyancy flux (free convection) as discussed earlier or by injecting lighter water with inflow velocity U_{in} through vertical opening d_{in} near the surface and withdrawing heavier water from below such that the net volume influx is zero (forced convection) as depicted in Fig. 21. Kao's (1980) similarity analysis suggests that U_{in} is related to the reduced gravity of the light water, g', and the volumetric discharge, Q_e, by $U_{in} = (g' Q_e)^{1/3}$. The conversion from the amount of fresher water supplied to the positive buoyancy flux (BF) is expressed in Qui *et al*, 1988 as:

$$BF = \rho_0 \beta \Delta s Q_e$$

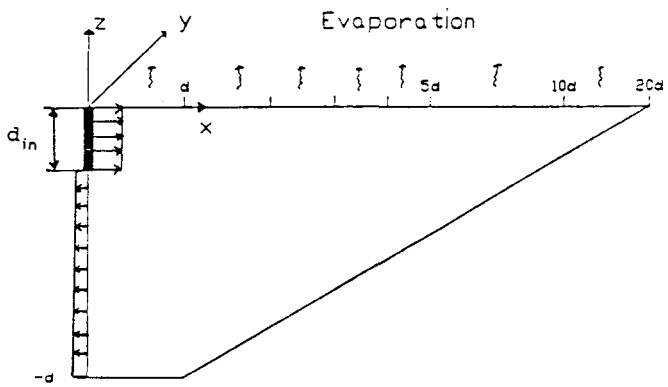

Fig. 21: The forced convection in the 2-D model.

where Q_e is the discharge of fresher water per unit length along the coast, ρ_0 is a reference density, β is the expansion coefficient for salinity and Δs is the salinity difference between the incoming freshner water and the ambient.

Two experiments are carried out to compare the two types of forcing. In each experiment, the model started at t = 0 and runs until t = 7, where t is in inertial days. All parameters are kept the same for the two cases except the boundary condition for the freshening process. The equilibrium solution for the two cases is reached after seven inertial days. The steady-state distributions of the isopycnals and the streamlines pattern for the free convection experiment are shown previously in Fig. 4 and Fig. 7, respectively. For the forced convection case, they are shown in Figs. 22 and 23.

The density fields are very similar in the two cases. The streamline patterns associated with each experiment are also very similar except near the vertical wall

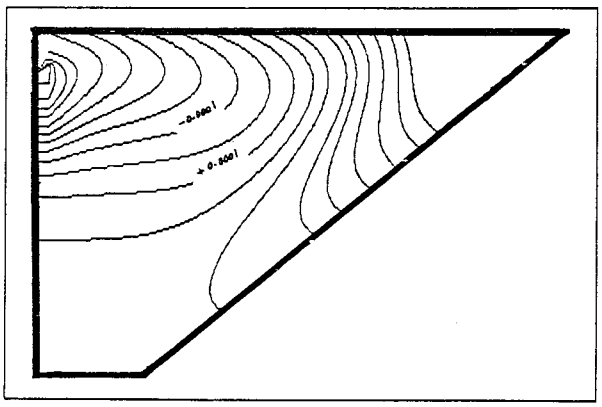

Fig. 22: Isopycnals for the forced convection ($\Delta\rho$ = .0001)

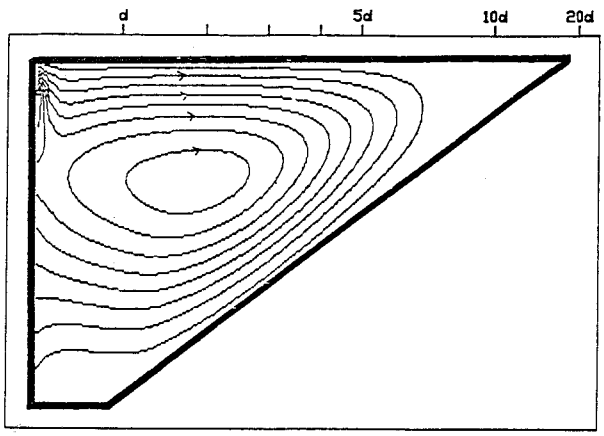

Fig. 23: Streamlines for the forced convection case ($\Delta\psi$ = 0.1)

where the streamfunction boundary conditions are different for each case. Along the vertical wall, the buoyancy influx induces upwelling in the free convection case, while in the forced convection case, downwelling prevails in a small localized region due to source-sink effect. The accumulation of isopycnals next to the wall in the free-convection experiment of Fig. 4 is due to this upward motion next to the wall. The prominent feature of the cross-sectional streamlines pattern is dominated by a clockwise convection cell, as shown in Fig. 23. These test experiments point out that the two types of forcing methods--salt efflux (buoyancy source) and buoyant inflow-outflow discharge--are analoguous in producing density fronts. Rouse, *et al,* 1952) pointed out the analogy for a point source, since it is the gravitational rather than the thermal aspect of the flow which is fundamental to the convection

phenomenon. Csanady 1982 pointed out the analogy in the oceanographic context using a linear model. This analogy will be exploited in forcing the 3-D model.

SUMMARY

A two-dimensional numerical study is undertaken here to investigate the cross-shore circulation dynamics of a rotating fluid dominated by surface evaporation. The major results of this study are as follows.

1. The driving forces in gravitational convection are the buoyancy influx and efflux of the fluid. The convection pattern can be obtained without regard to the specific means whereby the buoyancy effect is produced.

2. Applying the model to the Arabian Gulf, the vertical circulation induced by the density forcing alone in the f-plane of reference generates upwelling near the Iranian side and downwelling along the Arabian Gulf.

3. The density forcing alone produces a weak surface current of order 1 cm/sec in the upwind direction, and even weaker return-flow underneath. The addition of persistent wind field of a strength generally encounted in the winter months in the Gulf region enhances the transverse circulation pattern and completely reverses the direction of the surface alongshore flow, producing a downwind coastal jet over the shallow shelf with no coastal undercurrent. The windward surface current reaches 20 cm/sec, in agreement with field observations of surface velocity over the Arabian shelf (Picket, *et al,* 1984).

4. The dense water is formed over the shallow shelf by evaporation and migrates along the sloping topography toward the bottom of the deep channel. The bottom water formation is in agreement with field observations in the Gulf. The density structure is largely unaffected by wind forcing.

5. The critical wavelength during the onset of convection is about twice the maximum depth of the basin.

6. The vertical velocity induced by evaporation at the sea surface is proportional to Froude number or the buoyancy strength according to the relation:

$$W^* = 10^{-5} ((\Delta\rho/\rho_0)\ gd)^{1/2}$$

   For the Gulf basin, the vertical velocity induced by the average evaporation rate is of order 10^{-3} cm/s.

7. The steady state is achieved rapidly in a matter of seven days, driven through geostrophic adjustment and viscous and diffusive balances. In this 2-D study, 3-D transfer processes are precluded.

REFERENCES

1. **Al-Hajri, K., S.Y. Chao** and **T.W. Kao, 1991,** Circulation of the Arabian/ (Persian) Gulf: a three-dimensional model, (submitted to Journal of Geophysical Research).

2. **Brewer, P.G., A.P. Fleer, S. Kadar, D.K. Shafer** and **C.L. Smith, 1978,** Report A: Chemical oceanogrphic data from the Persian Gulf and Gulf of Oman, Woods Hole Oceanographic Institution Report, WHOI-78-37, Woods Hole, MA: p. 105.

3. **Csanady, G.T., 1982,** Circulation in the coastal ocean, Holland: D. Reidel Publishing Co., p. 279.

4. **Howard, L.N., 1964,** In the proceedings of the 11th International Congress of Applied Mechanics, Munich, 1964, H. Gortler editor, Springer, Berlin, 1110-1115.

5. **Ikeka, M., 1985,** Wind effects on a front over the continental shelf, Journal of Geophysical Research, 90 (C5), 9108-9118.

6. **Kao, T.W., 1980,** The dynamics of ocean fronts. I: the Gulf Stream, Journal of Physical Oceanogrphy, 10, 483-392.

7. **Kao, T.W., C. Park** and **H.P. Pao, 1978,** Inflows density currents, and fronts, Physics of Fluids, 21: 1912-1922.

8. **Piacsek, S.A., 1968,** Numerical experiments on convective flows in geophysical fluid systems, Proceedings of the 7th Naval Hydrodynamic Symposium, 4th ed., p. 753-784.

9. **Pickett, R.L., R.A. Pattridge, Arnone** and **J.A. Galt, 1984,** The Persian Gulf, oil and natural circulation, Sea Technology, 23:23-25.

10. **Porter, D.L., 1986,** Effects of a shelf break and of wind stress on the dynamics of oceanic fronts, Ph. D. thesis, The Catholic University of America, p. 174.

11. **Privett, D.W., 1959,** Monthly charts of evaporation from the north Indian Ocean, including the Red Sea and the Persian Gulf", Journal of Red Meteorological Society, 85:424-428.

12. **Purser, B.H., 1973,** The Persian Gulf. Holocene Carbonate Sedimentation and Diagenesis in a Shallow Epicontinental Sea, New York: Springer-Verlag, p. 471.

13. **Quon, C., 1987,** Nonlinear response of a rotating fluid to differential heating from below, Journal of Fluid Mechanics, 181:233-263.

14. Qui, B. and **N. Imasato, 1988,** Baroclinic instability of buoyancy-driven coastal density currents, J. Geophys. Res., 93, 5037-5050.

15. Roche, P.J., 1982, Computational fluid dynamics, Alguquerque, NM: Hermosa Publishers, p. 446.

16. Rouse, H., C.S. Yih and **H.W. Humphreys, Gravitational convection from a boundary source, Tellus, 4:201-210.**

17. Stern, M.E., 1975, Ocean Circulation Physics, New York: Academic Press, p. 143.

18. Sugimoto, T. and **J.A. Whitehead, 1983,** Laboratory models of bay-type continental shelves in the winter, Journal of Physical Oceanography, 13: 1819-1828.

19. Torrance, K.E. and **J.A. Rockett, 1969,** Numerical study of natural convection in an enclosure with localized heating from below: creeping flow to the onset of laminar instability. J. Fluid Mech. 36, 33-54.

20. Wright, J.L., 1974, A hydrographic and acoustic survey of the Persian Gulf, Part I, M.S. Thesis, Naval Postgraduate School, p. 47.